Acta Crystallographica Section D
Biological Crystallography
ISSN 0907-4449

X-ray crystallographic analyses of symmetrical allosteric effectors of hemoglobin: compounds designed to link primary and secondary binding sites

Martin K. Safo,[a]* Telih Boyiri,[b] James C. Burnett,[a] Richmond Danso-Danquah,[a] Carmen M. Moure,[c] Gajanan S. Joshi[d] and Donald J. Abraham[a]

[a]Department of Medicinal Chemistry, School of Pharmacy and Institute for Structural Biology and Drug Discovery, Virginia Commonwealth University, Richmond, Virginia 23298-0540, USA, [b]Division of Cancer Etiology and Prevention, American Health Foundation, Valhalla, New York 10595, USA, [c]Howard Hughes Medical Institute and Department of Biochemistry, Baylor College of Medicine, Houston, Texas 77030, USA, and [d]Allos Therapeutics Inc., 11080 CirclePoint Road, Suite 200, Westminster, Colorado 80020, USA

Correspondence e-mail: msafo@hsc.vcu.edu

Received 17 October 2001
Accepted 7 February 2002

PDB Reference: TB5-27–Hb, 1k0y, r1k0ysf.

The rational design and X-ray crystallographic analyses of two symmetrical allosteric effectors of hemoglobin (Hb) are reported. Compound design was directed by the previously solved co-crystal structure of one of the most potent allosteric effectors of Hb, 2-{4-[(3,5-dichlorophenylcarbamoyl)-methyl]-phenoxy}-2-methylpropionic acid (RSR4), which revealed two distinct binding sites for this compound in the Hb central water cavity. The primary binding site has been observed for all compounds of this structural class, which stabilize deoxy Hb by engaging in inter-dimer contacts with three of the four protein subunits. Interactions at the secondary binding site of RSR4 occur primarily between the β_1 and β_2 subunits and serve to further constrain the deoxy state. Based on these observations, it was hypothesized that compounds with the ability to simultaneously span and link both of these sites would possess increased potency, but at a lower molar concentration than RSR4. Two symmetrical compounds were designed and synthesized based on this hypothesis. The symmetrical effector approach was taken to minimize the number of compound orientations needed to successfully bind at either of the distinct allosteric sites. X-ray crystallographic analyses of these two effectors in complex with Hb revealed that they successfully spanned the RSR4 primary and secondary binding sites. However, the designed compounds interacted with the secondary binding site in such a way that intra-dimer, as opposed to inter-dimer, interactions were generated. In agreement with these observations, *in vitro* evaluation of the symmetrical effectors in Hb solution indicated that neither compound possessed the potency of RSR4. A detailed analysis of symmetrical effector–Hb contacts and comparisons with the binding contacts of RSR4 are discussed.

1. Introduction

Hemoglobin (Hb) is an allosteric tetrameric protein that exists in equilibrium between a low-affinity deoxy or tense state (T state) and a high-affinity oxy or relaxed state (R state). It is composed of two $\alpha\beta$ dimers, $\alpha_1\beta_1$ and $\alpha_2\beta_2$, which are geometrically related by a twofold axis of symmetry that intersects a central water cavity. The assembly of these dimers into a tetramer results in four intersubunit interfaces (α_1–α_2, β_1–β_2, α_1–β_2 and α_2–β_1). The T-state structure contains a wider central water cavity than the R-state structure and is preferentially stabilized by the indigenous allosteric effector 2,3-diphosphoglycerate (2,3-DPG) (a smaller water cavity in the R state precludes 2,3-DPG binding). This additional T-state stabilization shifts the Hb oxygen-equilibrium curve (OEC) to the right, resulting in enhanced oxygen delivery to the cardiovascular periphery. Synthetic allosteric effectors of

Hb have also been shown to bind exclusively within the central water cavity of the T state and to modify the allosteric properties of Hb in a physiologically similar fashion to 2,3-DPG (Abraham *et al.*, 1983, 1984; Perutz & Poyart, 1983). However, unlike 2,3-DPG, which binds in a 1:1 ratio with Hb, X-ray analyses of synthetic allosteric effector–Hb co-crystals have indicated that two or more of these molecules may bind simultaneously and in a symmetrically related fashion within the T-state central water cavity (Lalezari *et al.*, 1990; Randad *et al.*, 1991; Wireko *et al.*, 1991).

We have reported the high-resolution crystal structure of a potent synthetic allosteric effector, 2-{4-[(3,5-dimethylphenylcarbamoyl)-methyl]-phenoxy}-2-methylpropionic acid (RSR13) (Fig. 1), in complex with deoxy Hb (Safo *et al.*, 2001). Analysis of this co-crystal structure clearly indicated that two RSR13 molecules were bound in a symmetrically related fashion within the Hb central water cavity and that each engaged in equivalent inter-dimer interactions with three of the four protein subunits (Safo *et al.*, 2001). Recently, the X-ray co-crystal structure of an analog that is more potent (*in vitro*) than RSR13, 2-{4-[(3,5-dichlorophenylcarbamoyl)-methyl]-phenoxy}-2-methylpropionic acid (RSR4) (Fig. 1), revealed that four of these allosteric effectors can simultaneously bind in the Hb central water cavity (Moure, 1998). A comparison of the RSR13–Hb and RSR4–Hb complexes revealed that two of the bound RSR4 molecules superimpose on the RSR13-binding sites (referred to as the primary binding sites), while the other two RSR4 molecules bind to symmetrically equivalent secondary allosteric sites at the dimer–dimer interface (Lalezari *et al.*, 1990; Moure, 1998). The increased potency of RSR4 compared with that of RSR13 has been attributed to effector–Hb interactions at these secondary binding sites, which serve to further constrain the T state and subsequently enhance this molecule's ability to shift the OEC to the right.

This study focused on generating new allosteric effectors of Hb that would simultaneously interact with both the primary and secondary binding sites of RSR4. By spanning the two identified allosteric sites with a single molecule, it was hypothesized that the Hb-constraining inter-dimer interactions of two RSR4 molecules would be maintained by one compound, but at reduced molar concentration and with a decreased entropic binding penalty (*i.e.* the thermodynamic cost of binding one molecule to a protein is less than that of two molecules; Jencks, 1981). Using similar strategies, several research groups have shown that tethering small molecules, which bind to separate subsites on the same protein, can provide new ligands with enhanced activity. Shuker *et al.* (1996) have demonstrated the value of this technique in a study that generated nanomolar-range inhibitors of FK506 binding protein by tethering two millimolar-range inhibitors that were found to bind at proximal subsites. In another study, the same research group tethered two weak inhibitors of metalloproteinase stromelysin to generate a compound that inhibited in the nanomolar range (Hajduk *et al.*, 1997). Similarly, Burgess *et al.* (1999) tethered two weak inhibitors of human lung tryptase to generate a ligand with superior activity, while Maly *et al.* (2000) have developed nanomolar-range subtype-selective inhibitors of tyrosine kinase c-Src by tethering two compounds that were found to bind to different subsites of this enzyme.

Based on the RSR4–Hb co-crystal structure, two symmetrical compounds, 1,3-phenylene[bis(2-{4-[(aminocarbonyl)-methyl]phenoxy}-2-methylpropionic acid)] (TB5-27) (Fig. 1) and 1,3-{bis[2,2′-(2-{4-[(aminocarbonyl)methyl]phenoxy}-2-methylpropionic acid)phenoxy]}propane (TB5-39) (Fig. 1), which incorporated features of the basic RSR4 scaffold were designed and synthesized. The research in this paper focuses on the X-ray crystallographic analyses of these two effectors in complex with Hb. Importantly, the presented results demonstrate the usefulness of X-ray crystallography in the design of new therapeutic agents and set the stage for the future development of second-generation allosteric effectors of Hb.

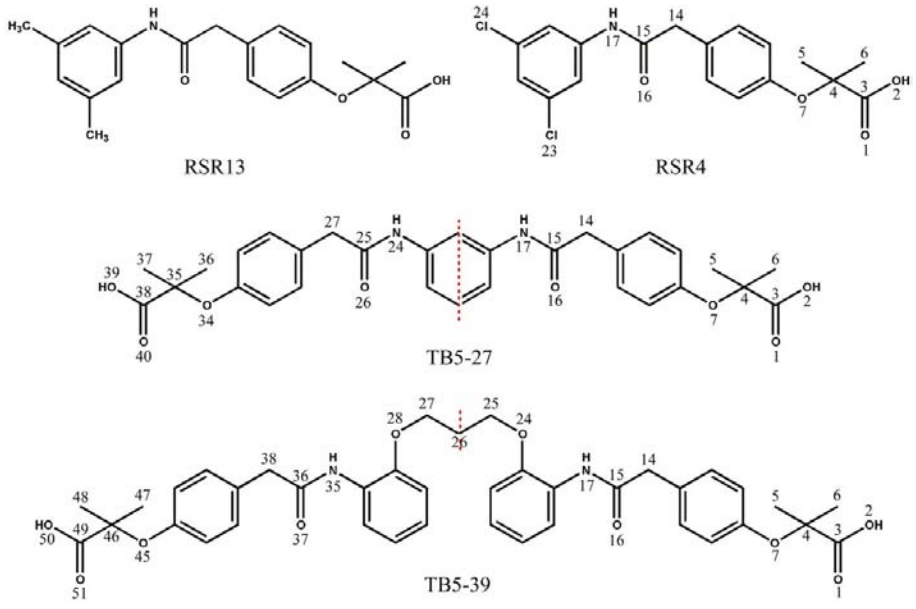

Figure 1
Two-dimensional structures of RSR13, RSR4, TB5-27 and TB5-39. Vertical dashed lines (red) indicate planes of symmetry.

2. Materials and methods

2.1. Crystallographic studies

Crystals of deoxy Hb–effector complexes (1:5 molar ratio) were grown from concentrated ammonium sulfate solutions using the batch method described by Perutz (1968). Both effector–Hb complexes were formed by combining 3.72×10^{-5} m*M* of the

Table 1
Crystallographic data and difference map statistics for TB5-27 and TB5-39.

Complex	TB5-27	TB5-39
Data-collection statistics		
Unit-cell parameters (Å, °)	a = 63.28, b = 83.7, c = 53.80, β = 99.33	a = 63.19, b = 83.20, c = 53.64, β = 99.34
Resolution (Å)	53.0–1.87 (1.94–1.87)	53.0–1.85 (1.90–1.85)
Observed reflections	119063 (8433)	184198 (12088)
Unique reflections	42624 (3287)	44031 (2927)
Completeness (%)	93.3 (73.8)	90.8 (79.6)
$R_{\rm merge}$†	4.8 (15.1)	5.4 (31.8)
Difference map statistics		
Resolution (Å)	20.0–2.0	20.0–2.0
No. of reflections	35537	35228
Rd-n‡	12.2	9.1

† $R_{\rm merge} = \sum(\langle I\rangle - I)/\sum I$. ‡ Rd-n is the agreement factor of structure amplitudes between native and derivative data.

Table 2
Refinement statistics for TB5-27.

Resolution (Å)	53.0–1.87 (1.96–1.87)
No. of reflections	42624 (4639)
R factor	16.3 (27.8)
$R_{\rm free}$	18.9 (29.2)
R.m.s.d. from ideal values	
Bond length (Å)	0.013
Bond angle (°)	1.73
Average B values (Å^2)	
All non-H atoms	22.0
Protein atoms	20.7
Heme atoms	18.9
Water atoms	37.5
Effector atoms	38.8
Estimated positional error (Luzzati)	
R factor†	0.19
$R_{\rm free}$†	0.22

† The R factor and $R_{\rm free}$ are based on 95 and 5% of the reflections used in the refinement, respectively.

respective effector with 7.44×10^{-6} mM oxygenated Hb. The crystallization setup was performed in a nitrogen-filled glove box (as described previously; Safo *et al.*, 2001). For both complexes, crystals suitable for data collection grew after 5 d.

X-ray diffraction data sets were collected at room temperature using Cu $K\alpha$ radiation on an R-AXIS IIC imaging-plate system which was mounted on a Rigaku RU-200 rotating-anode generator (operating at 50 kV and 180 mA). The space group was $P2_1$, with one molecule in the asymmetric unit. Diffraction data were collected to 1.87 and 1.85 Å for TB5-27 and TB5-39, respectively. The data were processed using the program *BIOTEX* from Molecular Structure Corporation (The Woodlands, Texas, USA) and scaled and averaged with the *CCP*4 suite of programs (Collaborative Computational Project, Number 4, 1994). Data-collection and processing statistics are summarized in Table 1.

2.2. Structure determination and refinement

The structure determination and refinement of RSR4 in complex with Hb is described elsewhere (Moure, 1998). The co-crystals of TB5-27–Hb and TB5-39–Hb were both isomorphous with the native deoxy Hb structure (Fermi *et al.*, 1984). Binding of both TB5-27 and TB5-39 to deoxy Hb was ascertained from difference Fourier electron-density maps computed from $F_{\rm obs}$(complex) − $F_{\rm obs}$(native) amplitude at 2.0 Å resolution, where $F_{\rm obs}$(complex) are the observed structure factors of the effector–Hb complexes and $F_{\rm obs}$(native) are the observed structure factors from the previously determined structure of native deoxy Hb (Fermi *et al.*, 1984). The agreement factor for the structural amplitudes between native and complex data (Rd-n) is reported in Table 1 at 2.0 Å. Models of the symmetrical allosteric effectors were built in *SYBYL* (version 6.4, Tripos Inc., St Louis, MO, USA) and were subsequently energy minimized using the Tripos force field. These models were fit to corresponding electron-density maps using *TOM-FRODO* (Cambillau & Horjales, 1987).

The TB5-27–Hb complex was refined using *X-PLOR* (Brünger, 1992*a*); attempts to refine TB5-39 bound at its allosteric site failed. The initial model used in refinement against the TB5-27–Hb diffraction data consisted of the native deoxy Hb coordinates without waters or sulfates. Topology and parameter files for TB5-27 were created based on the conformation of the effector in the difference electron-density map. All diffraction data were used in the refinement process and 5% of the reflections were set aside for the calculation of $R_{\rm free}$. The final structure-factor file contained anomalous differences and was used to refine the structure. A bulk-solvent correction was also introduced into the refinement. Rigid-body, positional and simulated-annealing refinements resulted in an R factor and $R_{\rm free}$ of 26.6 and 24.3%, respectively, for the structure (Brünger, 1992*b*). The allosteric effector coordinates were fit to the density maps and two sulfate ions and water molecules were also added to the model. The model was subjected to several alternate rounds of positional, simulated annealing and individual B-factor refinements and further addition of water. Manual adjustment of the model was intermittently performed with *TOM-FRODO*. Refinement statistics are reported in Table 2.

2.3. Synthesis

2.3.1. 2-{4-[(3-{2-[4-(1-Carboxy-1-methylethoxy)-phenyl]-acetylamino}-phenylcarbamoyl)-methyl]-phenoxy}-methyl-propionic acid (TB5-27). A mixture of 1,3-phenylenediamine (5.41 g, 50 mmol) and 4-hydroxyphenylacetic acid (15.22 g, 100 mmol) in *p*-xylene was refluxed for 48 h with the removal of azeotropic water from the reaction mixture. The intermediate, 1,3-phenylene{bis[4-(aminocarbonyl)methyl]phenol} (16.94 g, 90%), precipitated out of solution upon cooling of the reaction mixture. This product was filtered, washed with copious amounts of hexane and dried. The 1,3-phenylene{bis[4-(aminocarbonyl)methyl]phenol} intermediate (16.94 g, 45 mmol) was stirred in anhydrous dimethylformamide (40 ml) and reacted with ethyl α-bromoisobutyrate (23.4 g, 120 mmol) in the presence of anhydrous potassium carbonate (14.0 g, 100 mmol) at 353 K for 24 h. The mixture was cooled and diluted with water and diethyl acetate. The organic extract was dried over $MgSO_4$ and

evaporated to dryness to give the diester, 1,3-phenylene-[bis(ethyl-2-{4-[(aminocarbonyl)methyl]phenoxy}-2-methylpropionate)] (24.2 g), in 88.9% yield. 1,3-phenylene[bis(ethyl-2-{4-[(aminocarbonyl)methyl]phenoxy}-2-methylpropionate)] (24.2 g, 40 mmol) and 10% potassium hydroxide solution were added to ethanol/water (1:1) in a 100 ml round-bottom flask equipped with a magnetic stirrer. The mixture was stirred at room temperature for 2 h and the ethanol was removed under reduced pressure. The aqueous layer was diluted with water and neutralized with concentrated HCl. The precipitate was filtered and washed with water (200 ml) and then hexanes and oven dried to obtain 18.2 g of the title compound in 83% yield. Melting point, 474–475 K; ^{1}H NMR (DMSO-d$_6$) δ 9.40 (s, 2H, NH), 7.30 (s, 1H, ArH), 7.20 (d, 4H, ArH), 7.15 (d, 1H, ArH), 6.99 (d, 2H, ArH), 6.77 (d, 4H, ArH), 3.35 (s, 4H, ArCH$_2$), 1.41 (s, 12H, CH$_3$). Analysis: calculated for $C_{30}H_{32}N_2O_8.0.5H_2O$, C 64.62%, H 5.97%, N 5.02%; found, C 64.91%, H 6.31%, N 4.75%.

2.3.2. 2-[4-({2-[3-(2-{2-[4-(1-Carboxy-1-methyl-ethoxy)-phenyl]-acetylamino}-phenoxy)-propoxyl]-phenylcarbamoyl}-methyl)-phenoxy]-2-methylpropionic acid (TB5-39). A mixture of 2-nitrophenol (2.78 g, 20 mmol), 1,3-dibromopropane (2.02 g, 10 mmol), anhydrous potassium carbonate (3.0 g, 22 mmol) and acetone (100 ml) was stirred at reflux for 48 h. The reaction mixture was cooled and filtered and the solvent was removed by reduced pressure to obtain 1,3-[bis(2,2′-nitrophenoxy)]propane (2.83 g, 99% yield) as a pale yellow solid. The 1,3-[bis(2,2′-nitrophenoxy)]propane (2.83 g, 99 mmol) was dissolved in ethanol (100 ml) and hydrogenated in the presence of palladium-on-carbon catalyst (1.0 g) to afford 1,3-{bis(2,2′-aminophenoxy)}propane (2.52 g, 98% yield). A mixture of 1,3-{bis(2,2′-aminophenoxy)}propane (2.52 g, 9.8 mmol) and 4-hydroxyphenylacetic acid (2.98 g, 19.6 mmol) in *p*-xylene was refluxed for 48 h with the removal of azeotropic water from the reaction mixture. The intermediate, 1,3-{(bis{2,2′-[4-(aminocarbonyl)methyl]phenol})-phenoxy}propane (4.77 g, 91%), precipitated from solution upon cooling. This product was filtered, washed with copious amounts of hexane and dried. 1,3-{(bis{2,2′-[4-(aminocarbonyl)methyl]phenol})phenoxy}propane (4.77 g, 9.1 mmol) was stirred until dissolved in anhydrous dimethylformamide (40 ml) and was subsequently reacted with ethyl α-bromoisobutyrate (5.31 g, 27.2 mmol) in the presence of anhydrous potassium carbonate (3.5 g, 25 mmol) at 353 K for 24 h. The mixture was cooled and diluted with water and diethyl acetate. The organic extract was dried over MgSO$_4$ and evaporated to dryness to give the diester, 1,3-bis[2,2′-(ethyl-2-{4-[(aminocarbonyl)methyl]phenoxy}-2-methylpropionate)-phenoxy]propane (6.8 g) in 90% yield. To a 100 ml round-bottom flask equipped with a magnetic stirrer were added 1,3-bis[2,2′-(ethyl 2-{4-[(aminocarbonyl)methyl]phenoxy}-2-methylpropionate)phenoxy]propane (6.8 g, 9.0 mmol) and 10% potassium hydroxide solution in ethanol/water (1:1). The mixture was stirred at room temperature for 2 h and the ethanol was removed under reduced pressure. The aqueous layer was diluted with water and neutralized with concentrated HCl. The precipitate was filtered and washed with water (200 ml) and then hexanes and oven dried to obtain 5.1 g of the title compound in 70% yield. Melting point, 497–498 K; ^{1}H NMR (DMSO-d$_6$) δ 8.98 (s, 2H, NH), 7.85 (d, 2H, ArH), 7.21 (d, 4H, ArH), 6.997.10 (dt, 4H, ArH), 6.84 (d, 2H, ArH), 6.7 (d, 4H, ArH), 4.05 (t, 4H, OCH$_2$), 3.6 (s, 4H, ArCH$_2$), 2.10 (t, 2H, CH$_2$), 1.41 (s, 12H, CH$_3$). Analysis: calculated for $C_{39}H_{42}N_2O_{10}$, C 67.04%, H 6.06%, N 4.01%; found, C 67.10%, H 6.10%, N 4.09%.

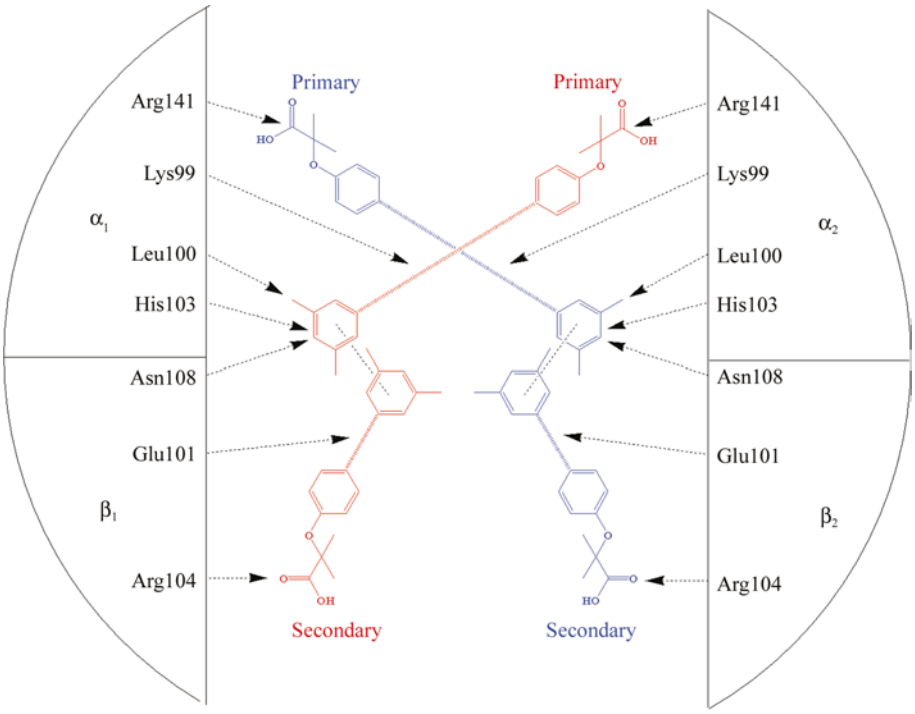

Figure 2
Two-dimensional schematic of important effector–residue interactions at the RSR4 primary and secondary binding sites. Arrows indicate effector–residue interactions and dotted lines indicate π stacking. RSR4 effectors are colored red and blue to indicate the desired binding mode of symmetrical effectors.

2.4. Hb oxygen-equilibrium studies

Purified stripped human adult Hb was prepared according to a previously described procedure (Randad *et al.*, 1991). Oxygen-dissociation curves were recorded on an AMINCO HEM-O-SCAN oxygen-dissociation analyzer (Travenol Laboratories). Compounds were dissolved in 50 m*M* HEPES buffer pH 7.4 to give 10 m*M* effector solutions. Immediately prior to running oxygen-dissociation curves, the Hb (5.4 m*M* in HEPES pH 7.4) and the test compounds were mixed in a 1:1 ratio (50 µl of Hb plus 50 µl of effector

solution) to give final concentrations of 2.7 m*M* of Hb and 5 m*M* of effector, with a molar ratio of 2:1 test compound to hemoglobin. Controls contained 50 µl of Hb in 50 µl HEPES buffer. Test samples were deoxygenated using nitrogen that contained 5% carbon dioxide. To measure the P_{50}, or the partial pressure of oxygen needed to saturate Hb, samples were saturated with 95% carbogen gas mixture (95% oxygen; 5% carbon dioxide). The oxygen pressure was gradually increased and the OEC was recorded from left to right. Hb saturation was recorded with a dual-wavelength spectrophotometer (577 and 586.2 nm). P_{50} was calculated by linear regression analysis from data points obtained between 40 and 60% oxygen saturation. Each effector was tested in duplicate with controls and the results accepted if the controls were within ±2 mmHg.

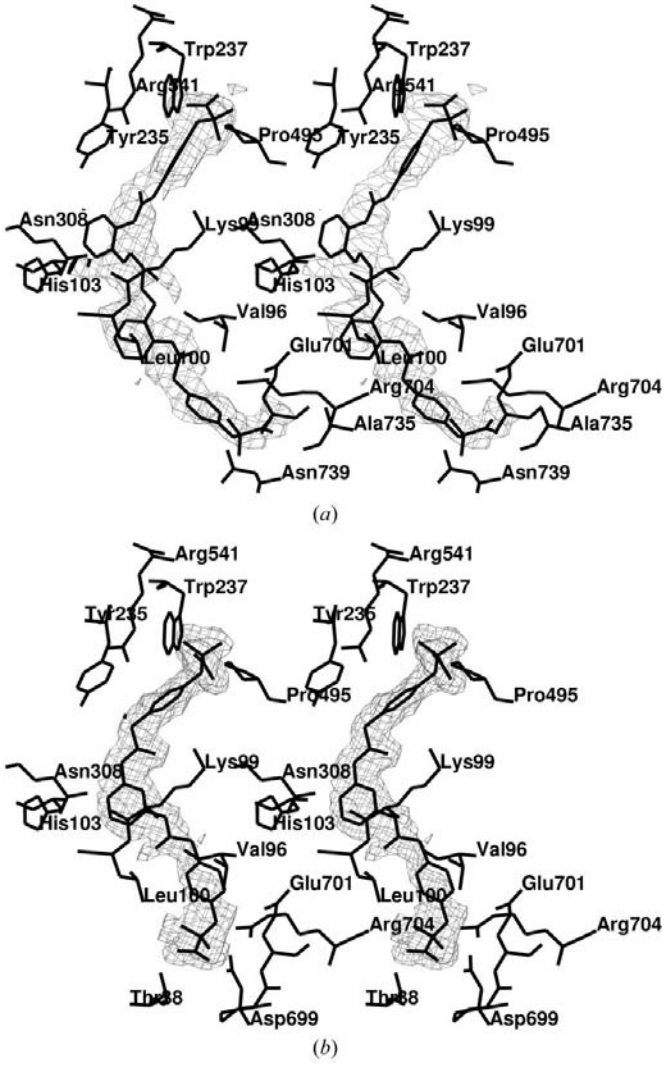

Figure 3
Stereoviews of (*a*) the $F_o - F_c$ density map of TB5-39 at the primary and secondary binding sites and (*b*) the $2F_o - F_c$ density map for TB5-27 at the primary and secondary binding sites. The maps are contoured at 2.66σ (*a*) and 0.92σ (*b*). In both (*a*) and (*b*) only one of two bound effectors in the central water cavity is shown; in each case symmetry-related binding is observed for the second bound effector. Both electron-density maps were generated with *TOM-FRODO* (Cambillau & Horjales, 1987).

3. Results

3.1. Design of symmetrical allosteric effectors

The RSR4–Hb co-crystal structure was used as a benchmark to design symmetrical allosteric effectors. Fig. 2 is a two-dimensional schematic diagram of important RSR4–Hb residue contacts in the primary and secondary binding sites. The primary binding site is located between the α_1–α_2 and α_1–β_2 subunit interfaces. The secondary binding site is located between the β1–β2 subunit interface. The rationale for designing symmetrical allosteric effectors was based on the premise that tethering two RSR4 molecules would generate an effector that could simultaneously interact with both the primary and secondary RSR4 binding sites and consequently constrain deoxy Hb as well as two separate RSR4 molecules, but at reduced concentration.

Binding-site interactions, effector orientations and distances between RSR4 molecules bound to the primary and secondary sites were used to design two *symmetrical* compounds, one rigid and one flexible (see Fig. 1). Both symmetrical compounds are basically two linked RSR4 scaffolds. Importantly, the 'symmetry' aspect of these molecules was incorporated to eliminate the need for a specific 'head-to-tail' binding orientation upon effector entry into the Hb central water cavity. Thus, it was rationalized that symmetrical molecules would bind to both the primary and secondary allosteric sites regardless of the 'portion' of the effector that entered the central water cavity first.

1,3-Phenylene[bis(2-{4-[(aminocarbonyl)methyl]phenoxy}-2-methylpropionic acid)] (TB5-27) is the more rigid of the two analogs (see Fig. 1). This effector possesses a plane of symmetry that bisects a central phenyl ring, and was designed based on the observation that the 3,5-dichloro-substituted phenyl rings of the RSR4 effectors at the primary and secondary sites are in close proximity to one another and engage in parallel π stacking. The more flexible analog, 1,3-bis[2,2′-(2-{4-[(aminocarbonyl)methyl]phenoxy}-2-methylpropionic acid)phenoxy]]propane (TB5-39) consists of two RSR4 scaffolds attached by a five-atom linker; a plane of symmetry bisects the central methylene of the five-atom tether. It was hypothesized that the flexibility of a five-atom bridge would allow any conformational adjustments that might be required for a symmetrical effector to simultaneously span both the primary and secondary sites.

3.2. Structural descriptions

Crystals of both effector–Hb complexes were isomorphous with the high-salt deoxy Hb structure described by Fermi *et al.* (1984). A difference Fourier electron-density map obtained with the phases of the deoxy Hb structure revealed two effectors bound to the central water cavity in a symmetry-related fashion for both complexes. Each bound symmetrical effector was observed to span both the primary and secondary

binding sites. The initial unrefined electron-density map for TB5-39 and the refined $2F_o - F_c$ electron-density map for TB5-27 are shown in Fig. 3. The electron density for TB5-27 is more ordered than that of TB5-39; for both complexes, effector primary-site electron density is more ordered than secondary-site density. Structure refinement with *X-PLOR* (Brünger, 1992*a*) was successful for TB5-27; however, owing to low effector occupancy, refinement of TB5-39 was not possible.

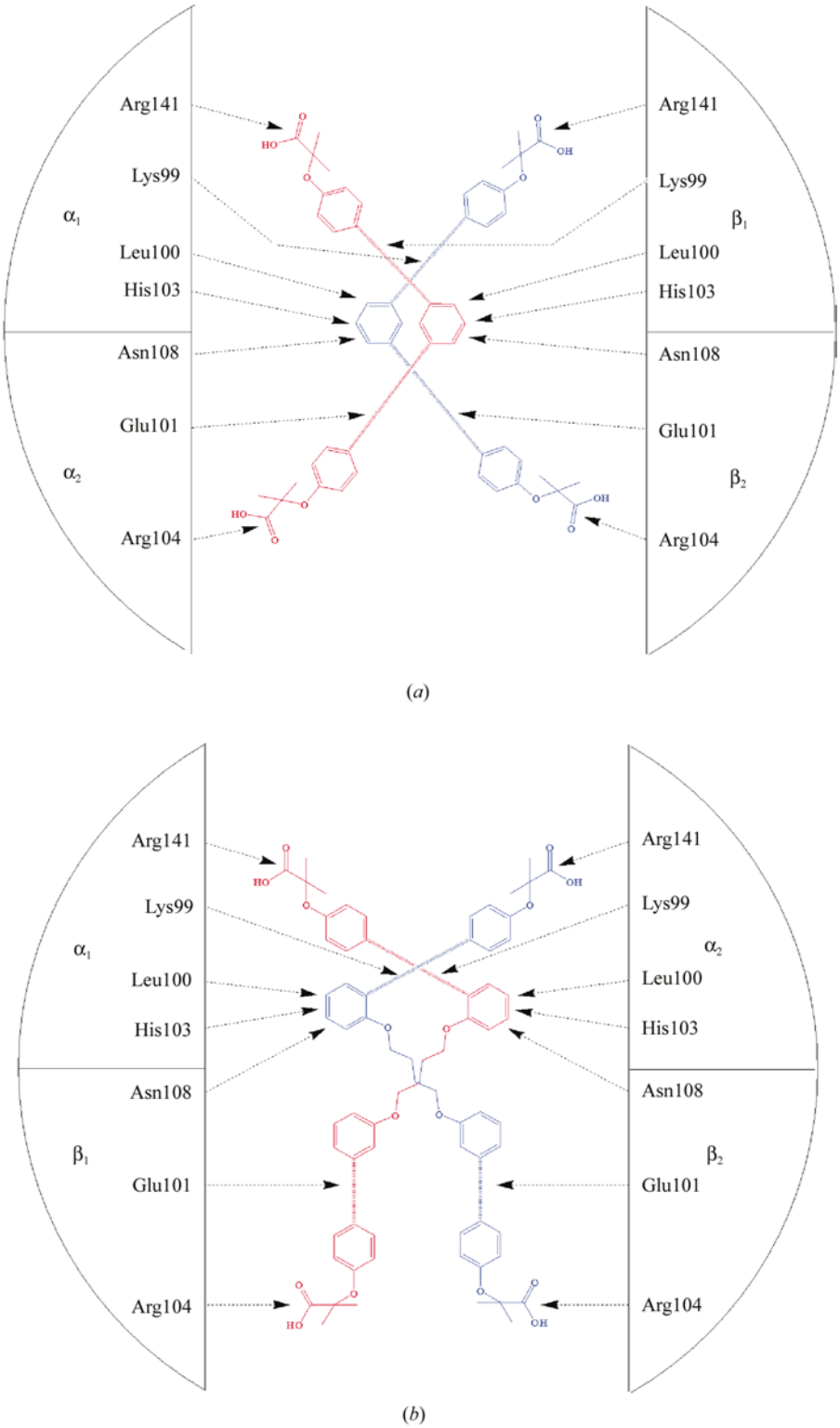

Figure 4
Two-dimensional schematics of contacts between (*a*) TB5-27 and Hb residues and (*b*) Tb5-39 and Hb residues. Red and blue effector molecules distinguish symmetrically related binding pairs. Black arrows represent important binding interactions between effectors and Hb.

The TB5-27–Hb complex was refined to an R factor of 16.3 and an R_{free} of 18.9% for all data to 1.87 Å resolution. The final model for the TB5-27–Hb complex consisted of 574 Hb amino-acid residues, four heme groups and 257 water molecules. Two sulfates were also identified in association with the β-subunits as described previously for RSR13 in complex with Hb (Safo *et al.*, 2001). Overall, the electron-density map of the TB5-27–Hb complex was very good, with only weak main-chain electron densities observed for N-terminal residues βVal1 and βHis2. Similar to the initial unrefined F_{obs}(complex) − F_{obs}(native) electron-density map, the $2F_o - F_c$ electron density at the TB5-27 primary site was clearly visible (with an average occupancy of 75% for the two primary site positions), while that of the secondary site was, by comparison, slightly less ordered (with an average occupancy of 50% for the two secondary-site positions).

The refined structure of the TB5-27–Hb complex was very similar to the native deoxy Hb structure as well as the RSR4–Hb co-crystal structure. A least-squares fit of all C^{α} in the TB5-27–Hb complex with those of the native deoxy Hb and the RSR4–Hb complex resulted in root-mean-square deviations (r.m.s.d.s) of 0.14 and 0.10 Å, respectively. Owing to weak electron densities, differences in the positions of residues β1Val1, β1His2 and β2Val1 were observed in all three structures.

The final models of both symmetrical effectors (in complex with deoxy Hb) contained two symmetrically related molecules bound in the Hb central water cavity. Furthermore, for all three effector–Hb complexes compared in this manuscript, RSR4, TB5-27 and TB5-39, interactions for each symmetrically related pair of bound effectors in each individual X-ray co-crystal structure are equivalent. Therefore, only one of each of the effectors in each of the symmetry-related pairs is

Table 3
Hydrogen bonds between RSR-4 and deoxy Hb/waters at the allosteric site.

Upper limit of hydrogen-bond contacts set to 3.6 Å.

RSR-4 atoms	Hb residue	Water	Distance† (Å)
RSR-4 primary binding site			
O1	α1Lys127 (O)	W1	3.3, 3.5
O2	α2Arg141 (OT1)	W2	3.4, 3.1
O2	α1Thr137 (O)	W2	3.3, 3.1
O16	β1Glu101 (OE2)	W3	3.3, 3.2
O16	α1Lys99 (NZ)		3.3
N17	β1Tyr35 (OH)	W4	3.3, 3,1
N17	β1Lys99 (O)	W5	2.8, 2.8
RSR-4 secondary binding site			
N17	β1Glu101 (OE1)		3.1
O1	β1Arg104 (NH1)		3.3
O2	α2Thr38 (OG1)		3.6

† For effector atoms hydrogen bonding with both residues and water, the distance to the protein residue is listed first and the distance to the water is listed second.

Table 4
Hydrogen bonds between TB5-27 and deoxy Hb/waters at the allosteric site.

Upper limit of hydrogen-bond contacts set to 3.6 Å.

TB5-27 atoms	Hb residue	Water	Distance† (Å)
O1	α1Lys99 (NZ)	W2	2.9, 3.3
O2	α2Arg141 (NE)	W1	2.8, 2.8
O7	α1Lys99 (NZ)	W2	2.9, 3.2
O16	α1Lys99 (NZ)		3.4
N17	β1Tyr35 (OH)	W4	2.9, 2.9
N17	β1Lys99 (O)	W3	2.8, 3.3
O34	β2Glu101 (OE1)		3.3
O34	β2Arg104 (NH1)		3.1
O39	β2Arg104 (NH1)		3.1

† For effector atoms hydrogen bonding with both residues and water, the distance to the protein residue is listed first and the distance to the water is listed second.

detailed in the text. In general, the primary-site interactions for both of the symmetrical effectors were comparable to those of RSR4; however, there were significant differences at the secondary binding sites: instead of the symmetrical effectors engaging in inter-dimer interactions at this location, as observed in RSR4, these compounds oriented in such a way that their secondary site methylpropionic acid moieties engaged in intra-dimer interactions (compare RSR4 binding in Fig. 2 with TB5-27 and TB5-39 binding in Figs. 4*a* and 4*b*). Specific atomic level effector–protein interactions will be discussed in detail for the TB5-27–Hb and RSR4-Hb complexes and, in general terms for TB5-39, which was not refined.

3.3. Comparison of symmetrical compound and RSR4 effector–deoxy Hb contacts at the primary binding site

Figs. 2 and 4 display two-dimensional contacts observed in the RSR4–Hb, TB5-27–Hb and TB5-39–Hb complexes; Fig. 5 displays three-dimensional contacts for each effector–Hb complex. Tables 3 and 4 detail specific hydrogen-bonding interactions between RSR4–Hb and TB5-27–Hb, respectively. Analysis of TB5-27 at the primary binding site indicates that the *gem*-dimethyl (atoms C5 and C6; see Fig. 1) of the methylpropionic acid fit into a hydrophobic cavity surrounded by residues α2Pro95, α2Thr137, α2Tyr140, α2Arg141 and β2Trp37 (Fig. 5*b*). In addition, the carboxylate of the methylpropionic acid (atoms C3, O1 and O2) engages in several water-mediated hydrogen bonds (Table 3) (water-mediated interactions will be detailed in a subsequent section). Based on the position of TB5-39 at the primary site, it appears that the *gem*-dimethyl portion (atoms C5 and C6) of this effector's methylpropionic acid moiety engages in similar but weaker hydrophobic interactions (Fig. 5*c*). Analysis of RSR4–Hb interactions at the primary site indicates that the *gem*-dimethyl portion (atoms C5 and C6) of this effector's methylpropionic acid engages in interactions that are comparable to those observed for TB5-27 (Fig. 5*a*). In addition, the carboxylate of the RSR4 methylpropionic acid (atoms C3, O1 and O2) is involved in water-mediated interactions that are markedly different from those observed in the TB5-27–Hb complex (Table 4).

The phenoxy rings (ring *A* in each effector; see Fig. 1) of both symmetrical effectors and of RSR4 engage in hydrophobic contacts with residues α1Lys99, β1Tyr35 and β1Trp37 at the primary site (Figs. 2, 4 and 5). Furthermore, the carbonyl O atom of the three-atom bridge in both TB5-27 (atom O16) and RSR4 (atom O16) is hydrogen bonded to the side-chain amine of α1Lys99 (Figs. 2, 4*a*, 5*a* and 5*b*). Based on the unrefined TB5-39–Hb complex it is not possible to accurately ascertain the interactions of this carbonyl O atom in the effector's three-atom bridge (Fig. 5*c*).

The TB5-27 central benzene ring (ring *B*) and the 3,5-dichloro-substituted benzene ring of RSR4 (ring *B*) share corresponding interactions at the primary site. Both effectors bind in a narrow hydrophobic pocket surrounded by residues α1Val96, α1Lys99, α1Leu100, α1His103, α1Phe36 and β1Asn108 (Figs. 2, 4*a*, 5*a* and 5*b*). Furthermore, the π electrons of this aromatic ring in both TB5-27 and RSR4 engage in hydrogen bonds with the side-chain amide N atom of residue β1Asn108. A similar interaction has been observed between the π electrons of the 3,5-dimethyl-substituted benzene ring of RSR13 and the side-chain amide N atom of β1Asn108 (Safo *et al.*, 2001). The corresponding aromatic ring (*B*) in TB5-39 adopts a different orientation compared with these moieties in TB5-27 and RSR4, but appears to maintain similar contacts (Figs. 4*b* and 5*c*). An important difference in binding between the symmetrical effectors and RSR4 results from the lack of 3,5-dichloro substitution on ring *B*. At the RSR4 primary binding site, one of the chloro substituents inserts into a hydrophobic pocket created by the G-helix residues α1Val96, α1Lys99, α1Leu100 and α1His103 (Fig. 5*a*). Owing to the absence of such substituents on corresponding aromatic rings in both TB5-27 and TB5-39, this hydrophobic insertion is not possible. In addition, the primary site 3,5-dichloro-substituted benzene of RSR4 also engages in π-stacking interactions with the 3,5-dichloro-substituted benzene ring of RSR4 bound at the secondary site (Figs. 2 and 5*a*).

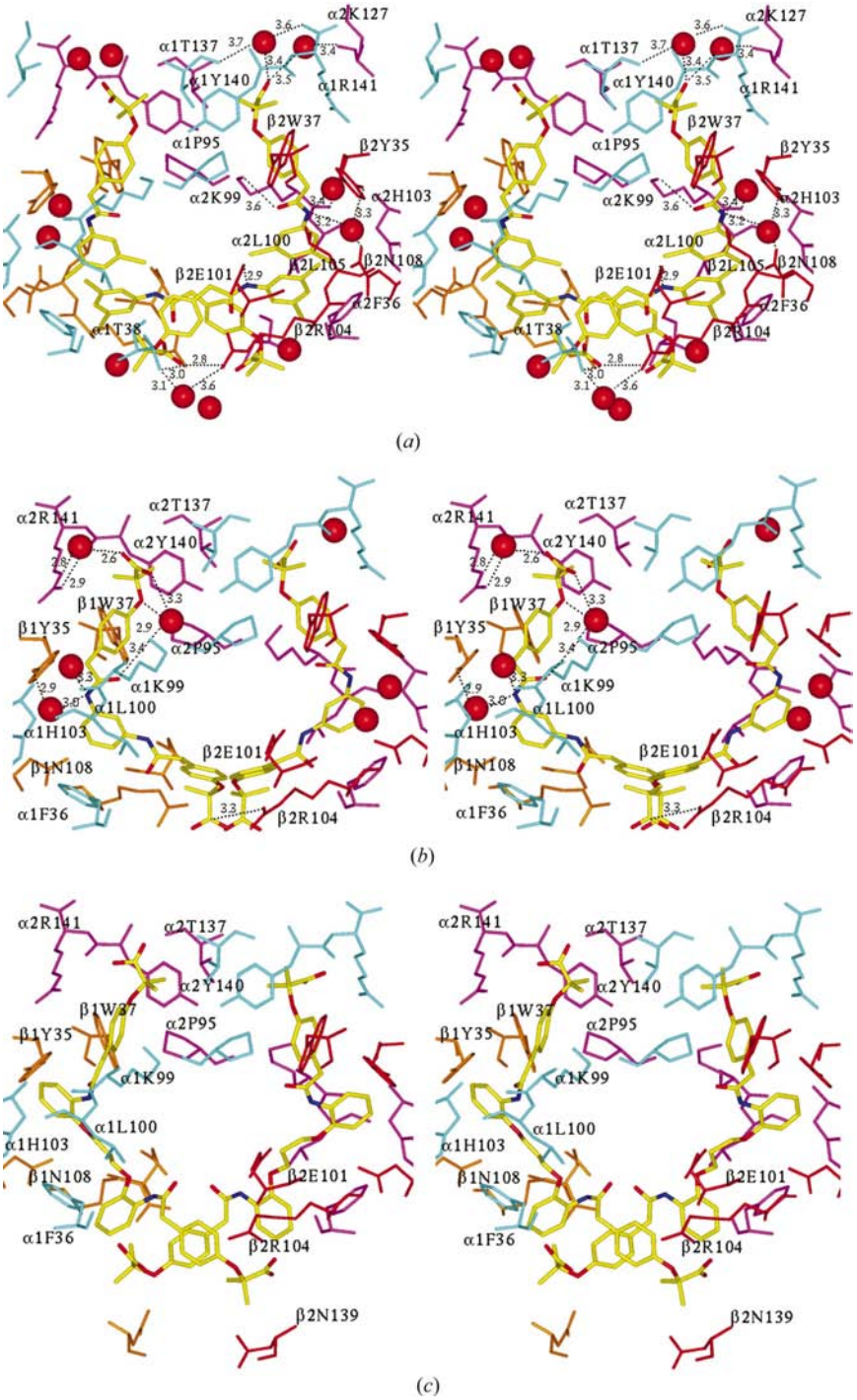

Figure 5
Stereoviews of allosteric sites of effectors (*a*) RSR4, (*b*) TB5-27 and (*c*) TB5-39. Protein and effector atoms are shown as sticks and structural waters are red spheres. The Hb α_1 subunit is light blue, the α_2 subunit is magenta, the β_1 subunit is orange and the β_2 subunit is red. C atoms of allosteric effectors are yellow, O atoms are red and N atoms are blue. Dashed black lines indicate hydrogen bonds. For clarity, not all Hb residues lining the allosteric binding sites are shown. Note, for visualization purposes, and owing to secondary-site binding orientation differences between RSR4 and the symmetrical effectors, Hb residue labels and interaction distances for RSR4 in Fig. 5(*a*) are labeled on the opposite side of the dimer–dimer interface with respect to labeled residues and interaction distances in the TB5-27–Hb complex (Fig. 5*b*) and the TB5-39–Hb complex (Fig. 5*c*). For clarity of description, textual reference to RSR4–Hb residue contacts follow dimer–dimer interface residue labeling as pictured for TB5-27 and TB5-39. Importantly, the described RSR4 interactions in the text correspond to equivalent interactions made by this effector at its symmetry-related binding sites and are the mirror image of the contacts labeled in Fig. 5(*a*)..

3.4. Comparison of symmetrical compound and RSR4 effector–deoxy Hb contacts at the secondary binding site

There are significant differences between RSR4 and symmetrical effector binding orientations and residue contacts at the secondary binding site. The secondary site methylpropionic acid of TB5-27 (atoms C38, O39 and O40) engages in an intra-dimer hydrogen bond with the side-chain guanidinium of β2Arg104 (Figs. 4*a* and 5*b*; Table 4). By comparison, the corresponding methylpropionic acid of RSR4 engages in an inter-dimer hydrogen bond with the side-chain guanidinium of residue β1Arg104 across the dimer–dimer interface (Figs. 2 and 5*a*; Table 3). Moreover, the methylpropionic acid moiety of RSR4 also hydrogen bonds with the side-chain hydroxyl group of α2Thr38 (Fig. 5*a*), while its three-atom-bridge N atom (N17) engages in a hydrogen bond with the side-chain carboxylate of β1Glu101 (Table 3). Owing to the length of TB5-39, this effector extends beyond the TB5-27 secondary binding site, and it appears that its methylpropionic acid moiety (atoms C49, O50 and O51) engages in a weak intra-dimer interaction with the side-chain guanidinium of β2Arg104 (Fig. 5*c*). This observation is corroborated by a comparatively weaker electron density for residue β2Arg104 at the secondary binding site in the TB5-39–Hb complex, indicating that the weak effector–residue interaction allows movement of the β2Arg104 side chain.

3.5. Comparison of structural waters at TB5-27 and RSR4 binding sites

Several structurally conserved water molecules mediate effector–Hb hydrogen bonds in both the TB5-27 and RSR4 complexes. At the primary binding site, the TB5-27 methylpropionic acid engages in two water-mediated hydrogen bonds: one with the side-chain guanidinium of α2Arg141 and one with the side-chain amine of α1Lys99 (Fig. 5*b*; Table 4). There is also a water-mediated hydrogen bond between the TB5-27 primary site phenoxy ether (atom O7) and the side-chain amine of α1Lys99 (Fig. 5*b*; Table 4). At the RSR4 primary binding site, the effector methylpropionic acid engages in water-mediated hydrogen bonds with the terminal carboxylate of α2Arg141, the backbone

carbonyl of α2Thr137 and the backbone carbonyl group of α1Lys127 (Fig. 5*a*; Table 3).

Two structurally conserved water molecules are located in close proximity to the three-atom-bridge amide N atoms of both TB5-27 (N17) and RSR4 (N17) at their primary binding sites. These two water molecules are also structurally conserved in the native deoxy Hb structure (Fermi *et al.*, 1984). In both TB5-27 and RSR4, one of these waters mediates a hydrogen bond with the side-chain phenol of residue β1Tyr35 (Figs. 5*a* and 5*b*; Tables 3 and 4). Furthermore, in the native deoxy Hb structure and the RSR4 and TB5-27 co-crystal structures these two waters are part of an extended structural water lattice that forms a network of intermolecular hydrogen bonds (Fermi *et al.*, 1984).

No water-mediated hydrogen bonds are observed at the secondary binding site in the TB5-27–Hb co-crystal structure (Fig. 5*b*). On the other hand, in the RSR4–Hb complex a structurally conserved water mediates hydrogen bonds between the side-chain hydroxyl group of α2Thr38 and the side-chain guanidinium of β1Arg104, both of which engage in direct hydrogen bonds with the carboxylate of the RSR4 secondary site methylpropionic acid (Fig. 5*a*). Thus, this structural water serves as the corner of a quadrilateral hydrogen-bonding network that serves to stabilize the binding mode of RSR4 at the secondary site.

3.6. Biological evaluation

The allosteric potencies of TB5-27, TB5-39 and RSR4 were evaluated as P_{50} measurements; P_{50} is the partial pressure of oxygen needed to half saturate Hb at 298 K and atmospheric pressure. Using a Hem-O-Scan, the P_{50} of native human adult hemoglobin is 19 mmHg ($\pm$ 1 s.d.). Allosteric effectors that stabilize deoxy Hb and subsequently decrease this protein's oxygen affinity increase the P_{50} relative to that of native Hb. The potency of each examined effector was measured as a ΔP_{50} value, which is the measured difference between Hb P_{50} in the presence and absence of the effector. ΔP_{50} values for TB5-27, TB5-39 and RSR4 were 41, 37 and 50 mmHg, respectively. Thus, all three effectors decreased the oxygen affinity of Hb by stabilizing the deoxy state; however, neither of the symmetrical effectors were as potent as RSR4. Hill coefficient (n_{50}) values for each effector were also calculated. The Hill coefficients for TB5-27, TB5-39 and RSR4 were 2.20, 2.32 and 2.01, respectively. By comparison, the average Hill coefficient for control samples was 2.5. Thus, these compounds had little effect on the cooperative nature of Hb.

4. Discussion

The high-resolution crystal structure of a potent allosteric effector of Hb (RSR4) revealed distinct primary and secondary allosteric binding sites and was subsequently used to design two symmetrical Hb effectors (TB5-27 and TB5-39) that would simultaneously interact with both of these sites. It was hypothesized that the two new compounds would be more potent than RSR4, as they would maintain the same important effector–Hb interactions, but at reduced molar concentration and with a decreased entropic binding penalty. *In vitro* biological evaluation of the symmetrical compounds indicated that both possessed very good potency with respect to the majority of allosteric effectors in this general structural class (Abraham *et al.*, 1992; Lalezari *et al.*, 1990; Randad *et al.*, 1991); however, neither symmetrical effector was as effective as RSR4. To link the biological activity of these two compounds to atomic level interactions, X-ray crystallographic analyses of TB5-27–Hb and T5-39–Hb co-crystals were performed. Comparison of symmetrical effector–Hb interactions with RSR4–Hb interactions indicated that differences in several key effector–residue contacts, as well as differences in effector–Hb water-mediated hydrogen bonds, accounted for observed differences in biological activity.

At the secondary allosteric site, structural analyses of both TB5-27 and TB5-39 in complex with deoxy Hb revealed a binding mode that differed from that of RSR4. When symmetry-related pairs of either TB5-27 or TB5-39 bind in the deoxy Hb central water cavity, the same binding space that is observed for two pairs of symmetry-related RSR4 molecules (*i.e.* one pair of RSR4 molecules bound to the primary sites and one pair of RSR4 molecules bound to the secondary sites) is covered. However, RSR4–Hb interactions at the secondary binding site are inter-dimer with respect to primary-site interactions, while symmetrical effector secondary binding site interactions are intra-dimer with respect to primary-site symmetrical effector–Hb interactions. Fig. 6 displays a stereo diagram of superimposed symmetry-related pairs of RSR4, RSR13, TB5-27 and TB5-39; note how primary binding site orientations are very similar for all effectors, while secondary-site orientations show that different binding modes have been adopted; the symmetrical effector's methylpropionic acid moieties turn towards the dimer on which the effector is primarily bound, while this functional group for RSR4 at the secondary site is extended across the dimer–dimer interface. Importantly, deoxy Hb is more constrained than oxy Hb owing to increased inter-dimer contacts across the dimer–dimer interface (Baldwin & Chothia, 1979; Bolton & Perutz, 1970; Kroeger & Kundrot, 1997; Shaanan, 1983); any effector that binds to the central water cavity of deoxy Hb and creates additional inter-dimer contacts will stabilize this allosteric state of the protein further (Abraham *et al.*, 1995, Boyiri *et al.*, 1995). RSR4 binds to the secondary site and contributes additional non-covalent binding interactions across the Hb dimer–dimer interface (Fig. 2); TB5-27 and TB5-39 bind at the secondary site, but do not add new non-covalent constraints to the Hb dimer–dimer interface (Fig. 4).

Interestingly, π stacking between the two 3,5-dichloro-subtituted benzene rings of RSR4 effectors bound at the primary and secondary sites appears to direct the binding orientation and subsequent residue contacts made by the methylpropionic acid moiety of this effector at the secondary site (Figs. 2 and 5*a*). Based on the activity of structurally similar Hb effectors that have been observed to bind only at the primary site (Safo *et al.*, 2001), and Hb solution binding-constant studies performed with RSR4 and similar allosteric

effectors (Abraham *et al.*, 1995), it is clear that RSR4 initially binds at the primary site. This is then followed by effector binding at the secondary site, and it is likely that the primary-site effector serves to direct the orientation of secondary-site binding by means of the intermolecular π-cloud stacking observed in the RSR4–Hb structure (Figs. 2 and 5*a*). By comparison, electron-density maps of the symmetrical effectors also suggest that these effectors bind with greater affinity at the primary site (Fig. 3). Thus, we predict that initial symmetrical compound binding takes place at the primary site and is followed by nesting of the rest of the molecule into the secondary site. However, in the symmetrical compounds there is no directionality imposed on the mode of secondary-site binding.

Another difference in RSR4 and symmetrical effector binding that appears to contribute to the observed disparity in potency between these compounds involves the 3,5-dichloro substituents on aromatic ring *B* (see Fig. 1) of RSR4. These substituents are not present in either TB5-27 or TB5-39. When RSR4 binds to the primary site, one of the 3,5-dichloro moieties of ring *B* inserts into a hydrophobic pocket of the G helix. This helix undergoes a rotation during the transition from the Hb deoxy to the oxy state (Baldwin & Chothia, 1979; Perutz & Fermi, 1993). Hence, the RSR4 chloro group that is inserted into this helix serves to interrupt this rotation and subsequently stabilizes the deoxy state. Analysis of the structurally similar allosteric effector RSR13 (in complex with Hb) corroborates this observation (Safo *et al.*, 2001). Furthermore, biological testing of numerous derivatives of RSR4 indicates that when an effector lacks hydrophobic substituents on aromatic ring *A,* or when at least one of the substituents on this aromatic ring cannot insert into the hydrophobic pocket of the G helix, a reduction in effector potency is observed (Randad *et al.*, 1991; unpublished observations). This observation, along with the intra-dimer *versus* inter-dimer binding mode of the symmetrical effectors at the secondary binding site, serves to partially explain, at an atomic level, why the two symmetrical compounds are not as active as either RSR13 or RSR4.

Differences in structural waters that mediate RSR4–Hb and symmetrical effector–Hb interactions also appear to contribute to differences in the allosteric activity of the examined compounds. In particular, analysis of the RSR4–Hb complex indicates that a water at the primary binding site mediates a hydrogen bond between the effector's methylpropionic acid carboxylate and the terminal carboxylate of α2Arg141; to date, this water-mediated interaction has not been observed in this structural class of effectors (Grella *et al.*, 2000; Safo *et al.*, 2001). Instead, a water-mediated interaction between the effector methylpropionic carboxylate and the side-chain guanidinium of α2Arg141 has been observed in analyzed effector–Hb co-crystals of this structural class. The TB5-27–Hb complex displays this mode of binding, with a structural water molecule observed to mediate hydrogen bonds between the effector methylpropionic acid carboxylate and the side-chain guanidinium of α2Arg141 (Fig. 5*b*). In native deoxy Hb, a strong hydrogen bond between the side-chain guanidinium of α2Arg141 and the side-chain carboxylate of α1Asp126 is important for stabilizing the deoxy state. The water-mediated hydrogen bond between the methyl propionic acid of TB5-27 and the side-chain guanidinium of α2Arg141 weakens the α2Arg141–α1Asp126 hydrogen bond, as it serves to buffer or 'soften' the original salt bridge. By comparison, the RSR4–Hb complex indicates that the α2Arg141 terminal carboxylate, and not the side-chain guanidinium, participates in a water-mediated hydrogen bond with the effector. Subsequently, the α2Arg141–α1Asp126 hydrogen bond is not disturbed when RSR4 binds at the primary allosteric site.

Another distinct difference in water-mediated hydrogen bonds occurs at the secondary binding site. In the RSR4 structure, a water molecule serves as part of a quadrilateral hydrogen-bonding network that links the effector methylpropionic acid carboxylate, the side-chain guanidinium of β1Arg104 and the side-chain hydroxyl group of α2Thr138 (Fig. 5*a*). By comparison, no water-mediated hydrogen bonds are observed at the TB5-27–Hb secondary binding site (Fig. 5*b*). Thus, the hydrogen bond between the TB5-27 methylpropionic acid carboxylate and the side-chain guanidinium of β1Arg104 is not reinforced, and is more transient than the same interaction observed in the RSR4–Hb complex.

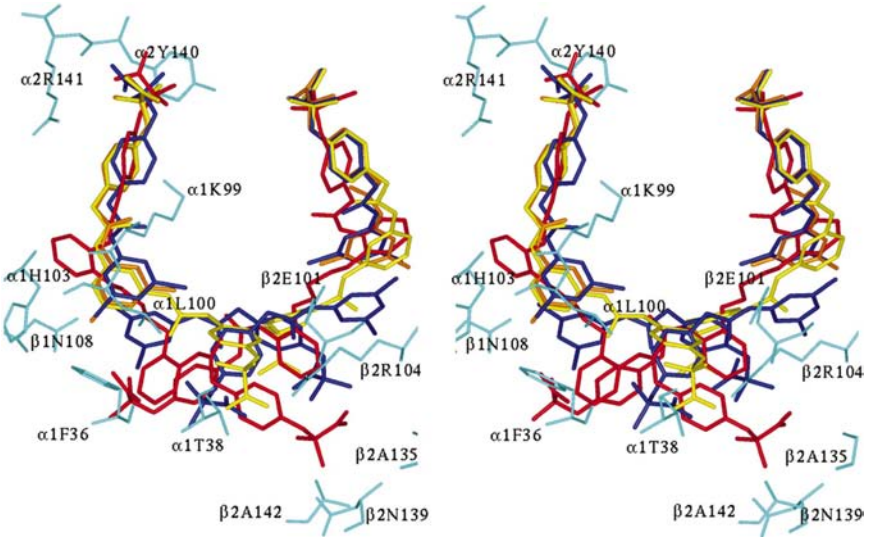

Figure 6
Stereoviews of symmetrically related pairs of allosteric effectors bound in the Hb central water cavity. Protein residues are shown as light blue sticks. RSR4 is blue, RSR13 is orange, TB5-27 is yellow and TB5-39 is red. Secondary-site binding for RSR4 is inter-dimer, while an intra-dimer binding mode is adopted by the TB5 compounds.

5. Conclusions

In these studies, X-ray crystallography has been used to (i) identify two separate Hb allosteric binding sites for the allosteric effector RSR4, (ii) direct the generation of symmetrical compounds designed to simultaneously span both of these distinct binding sites and (iii) verify the binding modes of these compounds and characterize their atomic level interactions with Hb residues and structural water molecules. Thus, these studies have clearly shown the value of X-ray crystallography at every level of ligand development from concept to design to verification.

Based on the analyzed co-crystal structures, a significantly more detailed understanding of the atomic level intermolecular interactions that lead to the allosteric modification of Hb by this class of effectors has been attained. It is now clear that effectors in the general 'RSR' structural class require a hydrophobic moiety that can insert into the Hb G helix (and thereby hinder the deoxy to oxy state transition) to achieve maximum potency, regardless of other new interactions that might be obtained at the expense of 'sacrificing' this interaction. Furthermore, these studies have provided new insights into the potential allosteric binding space that is available to this class of Hb effectors. In particular, this work indicates that it is possible to design allosteric effectors that will simultaneously bind to both the primary and secondary allosteric sites of Hb. Using the co-crystal structures of TB5-27 and TB5-39 as starting points, new allosteric effectors that will bind in an inter-dimer *versus* intra-dimer binding mode at the Hb secondary allosteric site will be designed. It is now evident that such compounds will require a 'directional' measure in their structure to ensure that they point across the Hb dimer–dimer interface. This may be achieved by incorporating a structural constraint such as a double bond in the bridge that tethers two 'RSR' scaffolds. Other strategies may involve varying tether lengths and composition, as well as adjusting the tether substitution patterns on the RSR scaffolds. Furthermore, future effectors designed to simultaneously bind at the primary and secondary sites will contain a hydrophobic substituent, such as a methyl or chloro moiety, that may insert into the Hb G helix. In fact, a combination of these modifications may be necessary to achieve enhanced effector potency.

This research was supported by grants from Allos Therapeutics, Inc. and from the National Institutes of Health Grants HL32793 (DJA) and HL04367 (MKS).

References

Abraham, D. J., Kennedy, P. E., Mehanna, A. S., Patwa, D. C. & Williams, F. L. (1984). *J. Med. Chem.* **27**, 967–378.
Abraham, D. J., Perutz, M. F. & Philips, S. E. (1983). *Proc. Natl Acad. Sci. USA*, **80**, 324–328.
Abraham, D. J., Safo, M. K., Boyiri, T., Danso-Danquah, R.E., Kister, J. & Poyart, C. (1995). *Biochemistry*, **34**, 15006–15020.
Abraham, D. J., Wireko, F. C., Randad, R. S., Poyart, C., Kister, J., Bohn, B., Liard, J. F. & Kunert, M. P. (1992). *Biochemistry*, **31**, 9141–9149.
Baldwin, J. & Chothia, C. (1979). *J. Mol. Biol.* **129**, 175–220.
Bolton, W. & Perutz, M. F. (1970). *Nature (London)*, **228**, 551–552.
Boyiri, T., Safo, M. K., Danso-Danquah, R. E., Kister, J., Poyart, C. & Abraham, D. J. (1995). *Biochemistry*, **34**, 15021–15036.
Brünger, A. T. (1992*a*). *X-PLOR Version* 3.840. *A System for X-ray Crystallography and NMR*. New Haven, CT, USA: Yale University Press.
Brünger, A. T. (1992*b*). *Nature (London)*, **355**, 472–475.
Burgess, L. E., Newhouse, B. J., Ibrahim, P., Rizzi, J., Kashem, M. A., Hartman, A., Brandhuber, B. J., Wright, C. D., Thomson, D. S., Vigers, G. P. A. & Koch, K. (1999). *Proc. Natl Acad. Sci. USA*, **96**, 8348–8352.
Cambillau, C. & Horjales, E. (1987). *J. Mol. Graph.* **5**, 174–177.
Collaborative Computational Project, Number 4 (1994). *Acta Cryst.* D**50**, 760–763.
Fermi, G., Perutz, M. F., Shaanan, B. & Fourme, R. (1984). *J. Mol. Biol.* **175**, 159–174.
Grella, M. P., Danso-Danquah, R., Safo, M. K., Joshi, G. S., Kister, M. M., Hoffman, S. J. & Abraham, D. J. (2000). *J. Med. Chem.* **43**, 4726–4737.
Hajduk, P. J., Sheppard, G., Nettesheim, D. G., Olejniczak, E. T., Shuker, S. B., Meadows, R.P., Steinman, G. M., Carrera, G. M. Jr, Marcotte, P. A., Severin, J., Walter, K., Smith, H., Gubbins, E., Simmer, R., Holzman, T. F., Morgan, D. W., Davidsen, S. K., Summers, J. B. & Fesik, S. W. (1997). *J. Am. Chem. Soc.* **119**, 5818–5827.
Jencks, W. P. (1981). *Proc. Natl Acad. Sci. USA*, **78**, 4046–4050.
Kroeger, K. S. & Kundrot, C. E. (1997). *Structure*, **5**, 153–311.
Lalezari, I., Lalezari, P., Poyart, C., Marden, M., Kister, J., Bohn, B., Fermi, G. & Perutz, M. F. (1990). *Biochemistry*, **29**, 1515–1523.
Maly, D. J., Choong, I. C. & Ellman, J. A. (2000). *Proc. Natl Acad. Sci. USA*, **97**, 2419–2424.
Moure, M. C. (1998). PhD Dissertation. Virginia Commonwealth University, Richmond, VA, USA.
Perutz, M. F. (1968). *J. Crystal Growth*, **2**, 54–56.
Perutz, M. F. & Fermi, G. (1993). *J. Mol. Biol.* **233**, 536–545.
Perutz, M. F. & Poyart, C. (1983). *Lancet*, **2**, 881–882.
Randad, R. S., Mahran, M. A., Mehanna, A. S. & Abraham, D. J. (1991). *J. Med. Chem.* **34**, 752–757.
Safo, M. K., Moure, C. M., Burnett, J. C., Joshi, G. S. & Abraham, D. J. (2001). *Protein Sci.* **10**, 951–957.
Shaanan, B. (1983). *J. Mol. Biol.* **171**, 31–59.
Shuker, S. B., Hajduk, P. J., Meadows, R. P. & Fesik, S. W. (1996). *Science*, **274**, 1531–1534.
Wireko, F. C., Kellogg, G. E. & Abraham, D. J. (1991). *J. Med. Chem.* **34**, 758–767.